Journal of Chromatography, 218 (1981) 97–122
Elsevier Scientific Publishing Company, Amsterdam — Printed in The Netherlands

CHROM. 14,090

DISPERSION OF PEAKS BY SHORT STRAIGHT OPEN TUBES IN LIQUID CHROMATOGRAPHY SYSTEMS

JOHN G. ATWOOD* and MARCEL J. E. GOLAY
The Perkin-Elmer Corporation, Main Avenue, Norwalk, CT 06856 (U.S.A.)

SUMMARY

The theory of spreading of a sample peak in a long straight open tube is known. However, when the tube becomes shorter than 30 theoretical plates, the eluted peak becomes non-gaussian and the theory for long tubes does not apply. This is the case for connecting tubes, injection loops and detector flow cells in liquid chromatographic (LC) systems. In earlier work, we studied the theory of this case using a computer model combining Poiseuille flow with diffusion, obtaining unexpected results about how samples wash out of short tubes. This work extends that study to obtain the peak shapes and bandwidths eluted from straight open tubes ranging from 0.01 to 30 plates in length.

An empirical expression was found for peak width which fits the results of the computer model to within 4% over this entire range. Below 3 plates, the normalized peak width is approximated by a constant times the inverse fourth root of normalized tube length in plates. It becomes as small as a quarter of the value predicted by the long tube theory for 0.01 plates. Experimental measurements on short tubes agree approximately with the computer model when diffusion is the only cause of radial mixing. An expression was derived which determines whether a tube is sufficiently straight so that secondary flow is unimportant compared with diffusion as a cause of radial mixing. Measurements on curved tubes are consistent with the expression. The conditions under which measurements of peak spreading in an open tube can be used to obtain the diffusivity of an LC sample are discussed.

A consequence of these results is that LC systems can be designed with substantially less bandwidth contribution from extra-column components than would be predicted using the long tube theory. Another consequence is that variances contributed by consecutive segments of short open tubes are not additive unless there is complete radial mixing at the connections between segments.

INTRODUCTION

The theory of dispersion of a sample peak injected into Poiseuille flow in a long straight tube is well known from the works of Taylor[1] and Golay[2]. When the tube is long there is ample time for radial diffusion to average each sample molecule's forward progress over the parabolic velocity distribution in the tube. The eluted peaks

0021-9673/81/0000–0000/$02.50

are gaussian in shape and the theory is in excellent agreement with experiments.

However, when the tube is short, or the diffusivity of the sample is low, or the flow-rate is high enough so that there is insufficient time for velocity averaging, the peak eluted from a small injection becomes markedly non-gaussian, and the theory for long tubes does not apply. This typically occurs for the connecting tubes, injection loops, and detector flow cells of liquid chromatography (LC) systems.

Gill and Ananthakrishnan[3] solved the convective-diffusion equations in a short tube and found that the peaks at the end of the tube may have double maximums. Golay and Atwood[4] studied this early phase of dispersion of the sample using a computer model combining diffusion and Poisseulle flow in an open tube with no retention. It was found that for the conditions typically encountered in LC systems, the shape of the peak eluted from the tube as a function of time depended only on the normalized length of the tube in theoretical plates, treating the tube as an open tubular column with zero retention[2]. The bandwidth of the eluted peak was proportional to tube volume, and when normalized by tube volume depended only on the normalized tube length in plates. It was found, surprisingly, that the washing out of the sample in the slowly moving layer near the tube wall occurred as a hump at the rear of an otherwise rectangular distribution along the length of the tube. This hump was shown by the computer model to cause a peculiar doubly curved shape in the peaks eluted from tubes shorter than 30 theoretical plates. Computer-calculated shapes of six peaks from tubes ranging from 30 down to 0.1 theoretical plates in normalized length were published, but no analysis of their bandwidths or variances was presented. Maycock *et al.*[5] solved the shape of peaks from tubes in the same range of normalized lengths by an entirely different numerical method and obtained results in general agreement.

This paper extends the earlier work as follows. Because some LC components such as detector flow cells may typically be as little as 0.01 theoretical plates in normalized length, the computer model was revised so that the calculation could be extended to tubes as short as this. Bandwidth and other properties of the peak shapes were calculated, and the way these properties vary with normalized length of the tube was studied. The purpose was to characterize these highly non-gaussian peaks so that more accurate estimates could be made of the bandwidth contributions of the components that produce them.

It was found that as the tube becomes longer than 3 plates, the normalized peak bandwidth, expressed as standard deviation, σ, divided by the tube volume, V_T becomes asymptotic to the inverse square root of normalized tube length as predicted by the theory for long tubes[1,2]. But as the tube becomes shorter than 3 plates, the normalized peak bandwidth becomes significantly smaller than predicted by the long tube theory. At 0.01 plates it is only one fourth as large.

A consequence of this result is that it appears possible to design LC components that make significantly less contribution to extra-column bandwidth than would be predicted using the long tube theory only.

Another consequence of the result is that the variances contributed by consecutive segments of short open tubes are not additive unless there is complete radial mixing at the connection between the segments.

Several experiments are described which tend to verify the correctness of the computed results, yet show the limits of their applicability. The principal limitation is

that in the theory for laminar flow in straight tubes, diffusion is the only cause of radial mixing. Therefore, any experiments to be governed by such a theory must be free of the radial mixing effects of secondary flow such as is caused by curved tubing paths or abrupt changes in cross section. It was found necessary in the experiments to keep tubes surprisingly straight to get results in agreement with the theory, except at very low flow-rates. A simple expression was derived from the work of Golay[6] which determines in advance whether a tube is sufficiently straight so that secondary flow is unimportant compared with diffusion as a cause of radial mixing. Measurements of peak dispersion made in a curved tube are consistent with this expression. Many other predictions of the theory remain to be tested experimentally, however.

THEORY

A straight open tube can be treated as an open tubular column without retention[2]. It has an optimum velocity at which the height of a theoretical plate is minimum. Multiplying the expression for the optimum velocity by the area of the tube's cross-section gives the corresponding optimum flow-rate, F_{opt} as

$$F_{opt} = \sqrt{48}\,\pi D r_0 \tag{1}$$

where D is diffusivity of the sample in the mobile phase and r_0 is the inside radius of the tube. For a typical sample with $D = 10^{-5}$ cm^2/sec in a tube with 0.009 cm radius, $F_{opt} \approx 2 \cdot 10^{-6}$ cm^3/sec, or roughly 10^{-4} ml/min. Thus, the flow-rates in typical LC systems are of the order of 1000 to 10,000 times the optimum flow-rates in the connecting tubes. Even for detector cells with 0.025 cm radius, $F_{opt} \approx 3 \cdot 10^{-4}$ ml/min, so that a flow-rate of 10 μl/min, as is typically used with microbore columns[8] is about 30 times F_{opt}. Under these conditions, except for a brief instant at the start, convection due to Poiseuille flow is always far more important than longitudinal diffusion as the cause of axial dispersion of the sample and we may use only the dynamic diffusion term of the expression for plate height, h, in the tube. Expressed in terms of flow-rate, F, it is

$$h = F/24\,\pi D \tag{2}$$

Using this expression we can determine the number of theoretical plates, n, in a tube of length L:

$$n = L/h = 24\,\pi D L/F \tag{3}$$

For long tubes where $n > 30$, the shape of the eluted peak is very close to gaussian, and its variance, σ^2, is the familiar

$$\sigma^2 = V_T^2/n \tag{4}$$

where V_T is the volume of the tube, and the standard deviation is expressed in units of volume.

Ref. 4 shows that as n decreases below about 30, the eluted peak becomes

increasingly non-gaussian and the assumptions under which eqn. 4 is derived become less and less true. It is then necessary to compute the shape of the eluted peak from a numerical computer model.

It is sufficient for typical LC systems to compute the eluted peak shape for each tube length at only one flow-rate. Referring to Figs. 6 and 8 of ref. 4, and noting that $F/F_{opt} = v_0/v_{opt}$ (where v_0 and v_{opt} are the average flow velocity and the optimum flow velocity, respectively) it is clear that the variance and skewness of the sample distribution inside the tube are almost independent of flow-rate when $F/F_{opt} \geqslant 30$, even when the average flow has traveled only 0.015 theoretical plates. This is the earliest event observable in this computer model. It is a single iteration. Thus, it is justifiable to use peak shapes calculated for $F/F_{opt} = 100$ as reasonably representative for all flow-rates such that $F/F_{opt} \geqslant 30$, the range of interest for short tubes in LC systems.

THE NUMERICAL COMPUTER MODEL

The model used to calculate the peak shapes is described in detail in ref. 4. Briefly, it divides the tube into volume elements consisting of 20 concentric rings at equal increments of radius and slices at equal increments of length along the tube. Poiseuille flow is simulated by advancing the sample in each volume element along the tube according to the velocity at that radius. Diffusion is simulated by redistributing part of the sample in each volume element to the elements adjacent to it. One cycle of simulated flow followed by simulated diffusion is defined as one iteration and corresponds to the time unit in the model. Sample injection is simulated by starting with an initial sample in all the rings of the first slice of the tube. Thousands of iterations over tens of thousands of volume elements simulate the combination of Poiseuille flow with diffusion which disperses the sample in the tube. The model can be asked to describe the distribution of sample along the tube after a certain time, or the sample content in all the rings of a certain slice as a function of time, or the rate of elution of sample from a tube of a certain length as a function of time.

After a sufficient number of iterations, the sample is smoothly distributed over a large number of volume elements, and the model can be expected to simulate the physical process with very great accuracy. However, it can be seen by referring to Fig. 5 of ref. 4 that for $F/F_{opt} = 100$, it takes only 3 iterations for the sample to reach the end of a tube 0.1 plates long, and the computed distribution of sample still shows substantial effects from the discreteness of the model.

Therefore, to study peak shapes eluted from tubes as short as 0.01 theoretical plate, it was necessary to modify the computer model to give it a finer grid in space and time. This was done by changing the number rings into which the tube was subdivided from 20 to 50. This raised the iterations per theoretical plate from 66.67 to 416.67. In the 50-ring model, the sample reaches the end of a tube 0.01 plates long at the second iteration.

Both models become increasingly accurate after several iterations because the width of the features being measured becomes larger than a few slices. These conditions, however, do not apply for the initial onset and rapid drop at the start of peaks where $n \leqslant 0.3$ plates. The accuracy of computer-calculated properties such as width at half height and retention volume at the peak maximum are thus visibly affected by the coarseness of the grid of the models. Fortunately, for these limiting cases, reliable

simple theory of dispersion by Poiseuille flow without diffusion indicates the correct limiting values.

In this work, data for normalized tube lengths of 0.3–30 plates were calculated using the 20-ring model of ref. 5. For normalized tube lengths from 0.1 to 0.01 plates the 50-ring model described above was used. For a normalized tube length of 0.1 plate, the two models agreed as to standard deviation of the eluted peak to within 1.5%. This small discrepancy is believed to be caused in part by the fact that at 0.1 plate, the 20-ring model's accuracy is slightly affected by having an insufficient number of iterations at the onset of the peak to average out the discreteness of the model.

The calculated peak shapes were processed by another program which determined the location of the peak maximum, the location of the centroid, the standard deviation, and the minimum width containing 95% of the peak's area. Since this program was designed to process relatively noisy experimental data, its accuracy in calculating standard deviation of the computed peaks is estimated to be about 0.5%.

COMPUTED RESULTS

Elution peak shapes

Elution is the average concentration of sample in the fluid leaving the end of a tube as a function of time, after a very narrow injection uniformly across the entrance to the tube. It is the signal that would be seen by a detector with very small volume that mixes together the fluid from all parts of the end of the tube and responds to the instantaneous concentration that results.

Fig. 1 shows the peak shapes eluted from tubes from 0.01 to 30 plates in length.

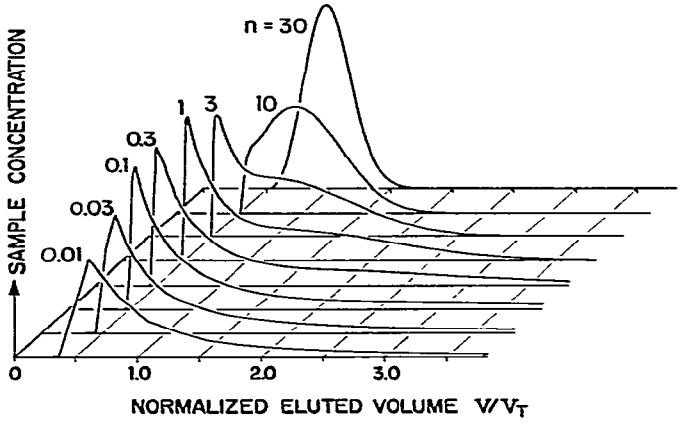

Fig. 1. Elution peak shapes as a function of normalized tube length, n, in plates. Eluted sample concentrations from numerical computer model are normalized to represent injections of a small, constant sample mass into tubes of constant volume V_T and plotted *versus* normalized eluted volume V/V_T. When $n < 0.3$ plates, the true peak shape has an almost instantaneous onset and peak maximum at $V/V_T = 0.5$. Sloping onsets and angularity of the computed curves for these values of n are caused by coarseness of the model for very early events. Transition from the short-tube peak shape to gaussian peaks for long tubes as n increases can be seen to occur by the development of a hump which moves in from the tail to a normalized retention volume of 1.0, where it grows and narrows to become the main peak.

Sample concentration in arbitrary units is plotted *versus* normalized eluted volume, V/V_T, where V is the volume eluted since the time of injection. Each peak computed by the model is normalized by dividing its abscissa scale by the length of the tube in theoretical plates. Thus, each curve represents elution from a tube of unit volume. Each ordinate scale is adjusted so that all curves have the same area. Thus the curves simulate an experiment in which a sample of fixed mass and very small volume is injected into a tube of fixed volume whose length in theoretical plates is varied by changing the flow-rate or sample diffusivity.

When $n < 0.3$, the Poiseuille velocity profile should result in each peak having a very abrupt onset at $V/V_T = 0.5$, followed by a hyperbolic decay proportional to $(V/V_T)^{-2}$ in the early stages. The results show this only approximately. The sloping onset for the shortest tubes is attributable to the aforementioned coarseness of the model grid for the earliest stages of dispersion.

As shown in ref. 4, the hyperbolic tail of each peak is truncated by combined radial diffusion and velocity shear. This sweeps the sample at the walls ahead as a "hump" of concentration which accelerates until it catches up with the average flow in the tube. This hump can be seen in the curves of Fig. 1 moving in from near $V/V_T = 8$ when $n = 0.01$ toward $V/V_T = 2$ at $n = 0.3$. Finally, for $n \geqslant 3$, the hump becomes the main peak at $V/V_T = 1.0$. The onset peak at $V/V_T = 0.5$ finally disappears at $n = 30$ as diffusion destroys the sharp front on the axis of the tube and the eluted peak approaches a gaussian shape. For $n \geqslant 30$ the longitudinal sample distributions at all radii in the tube are close to being gaussian, with the distribution on axis leading the distribution at the wall by 3 theoretical plates, and the eluted peaks are very close to gaussian.

Table I gives quantitative data on the persistence of the tails on elution peaks from short tubes. The first four columns give the number of tube volumes that must be eluted before the concentration drops below 10, 1 and 0.1 % of its peak value, as a function of normalized tube length, n.

TABLE I

LENGTHS OF TAILS OF ELUTION AND SLICE CONTENT PEAKS IN TERMS OF NORMALIZED ELUTED VOLUMES, V/V_T TO ATTAIN CONCENTRATIONS LESS THAN 10, 1 AND 0.1 % OF PEAK CONCENTRATION

Normalized tube length, plates	*Elution peaks*			*Slice content peaks*		
	V/V_T for these percents of peak concentration:			*V/V_T for these percents of peak concentration:*		
	10	*1*	*0.1*	*10*	*1*	*0.1*
0.01	2.1	8.6	15.4	9.4	16.5	22.6
0.03	1.9	7.5	10.9	7.2	11.1	13.8
0.10	1.7	5.8	7.5	5.4	7.5	8.8
0.30	2.3	4.6	—*	4.2	5.5	—*
1.0	2.4	3.4	—	3.1	3.9	—
3.0	2.1	2.7	—	2.4	2.9	—
10	1.7	2.1	—	1.8	2.3	—
30	1.4	1.6	—	1.4	1.6	—

* Data not available from peaks computed with the 20-ring model.

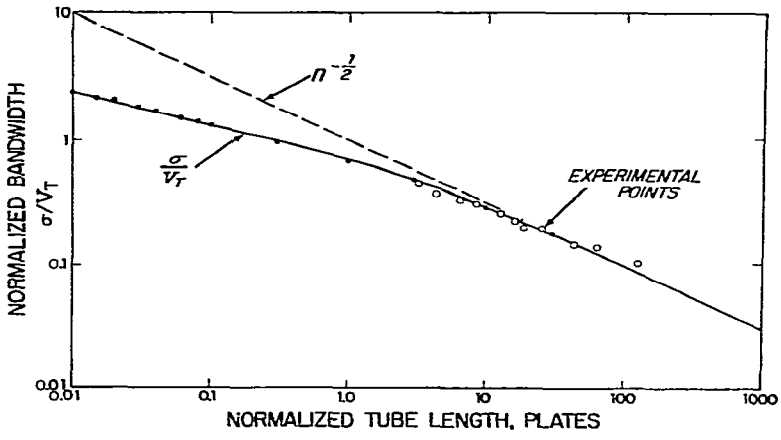

Fig. 2. Elution bandwidth *versus* tube length on log–log scales. Normalized standard deviation σ/V_T *versus* normalized tube length n in plates for the peak eluted from a straight open tube. Solid dots are values from the numerical computer model. The solid line is from eqn. 5. Open circles are means of measurements on a straight stainless-steel tube (366 cm × 0.41 mm I.D.) where flow-rate was varied from 4.2 to 0.105 ml/min to vary the normalized tube length. Sample was sodium benzoate in water at room temperature. Broken line shows extension of $n^{-1/2}$ asymptote which applies for $n > 30$.

Elution bandwidth

Fig. 2 shows a log–log plot of the normalized standard deviation, σ/V_T, of eluted peaks *vs.* tube length in plates. It shows that for $n > 3$ plates, σ/V_T is asymptotic to $n^{-1/2}$, in expected agreement with the theory for long tubes. For $n < 3$ plates, σ/V_T has a continually decreasing slope indicating that it is approximately proportional to $n^{-1/4}$. It can be seen that when $n < 10$, significant errors in calculation of σ result if the long-tube formula is used.

Table II gives some properties of the computed peak shapes for 13 different normalized tube lengths. The second column gives the normalized standard deviation, σ/V_T. An empirical expression was found that closely approximates these computed values down to $n = 0.01$ plates. It is

$$\sigma/V_T \approx n^{-1/2}(1 + 3/n)^{-1/4}, \qquad n \geqslant 0.01 \tag{5}$$

The third column of Table II gives the ratio of this approximate expression to the computed σ/V_T. It shows that the maximum error of the approximation is 3.8%. Thus, for many purposes, eqn. 5 has adequate accuracy within its range down to $n = 0.01$. The empirical character of this equation must be emphasized: theoretical considerations indicate that for indefinitely decreasing values of n, σ/V_T approaches a constant times $n^{-1/6}$.

To measure the true σ of non-gaussian peaks in experimental work involves substantial computation. Therefore it is of interest to see how the commonly used simpler methods of estimating σ perform for the particular non-gaussian shapes which occur for $n = 30$. One such measure is width at half height, $W_{1/2}$, which equals 2.355 σ for a gaussian peak. The fourth column of Table II gives the ratio $W_{1/2}/2.355\ \sigma$. A similar measure also used is width at 0.6067 of peak height, $W_{0.6}$ which equals 2σ

TABLE II

PROPERTIES OF THE PEAK SHAPE ELUTED FROM A SHORT STRAIGHT TUBE AS A FUNCTION OF TUBE LENGTH IN THEORETICAL PLATES

Normalized tube length in plates, n	*Normalized standard deviation from computer,* σ/V_T	*Ratio of approximate formula to normalized standard deviation from computer,* $n^{-1/2}(1 + 3/n)^{1/4}/(\sigma/V_T)$	*Ratios of other bandwidth measures to standard deviation*			
			Width at half height, $W_{1/2}/2.355\sigma$	*Width at 0.6066 of height* $W_{0.6}/2\sigma$	*Width containing 0.9546 of peak area* $W_{0.95}/4\sigma$	*Normalized centroid,* V_c/V_T
0.010	2.453	0.980	0.0849	0.0696	0.772	2.016
0.015	2.176	0.997	0.0838	0.0752	0.797	1.914
0.020	2.009	0.971	0.0857	0.0776	0.802	1.853
0.030	1.846	0.986	0.0812	0.0682	0.790	1.824
0.040	1.702	0.995	0.0804	0.0666	0.788	1.757
0.060	1.522	1.004	0.0772	0.0646	0.789	1.677
0.080	1.418	1.001	0.0849	0.0765	0.787	1.639
0.10	1.332	0.994	0.0846	0.0707	0.786	1.597
0.30	0.965	1.038	0.121	0.108	0.785	1.387
1.0	0.688	1.029	0.148	0.127	0.767	1.259
3.0	0.480	1.011	0.338	0.221	0.810	1.134
10.0	0.297	0.997	1.18	1.21	0.898	1.034
30.0	0.179	0.997	1.05	1.05	0.978	1.011

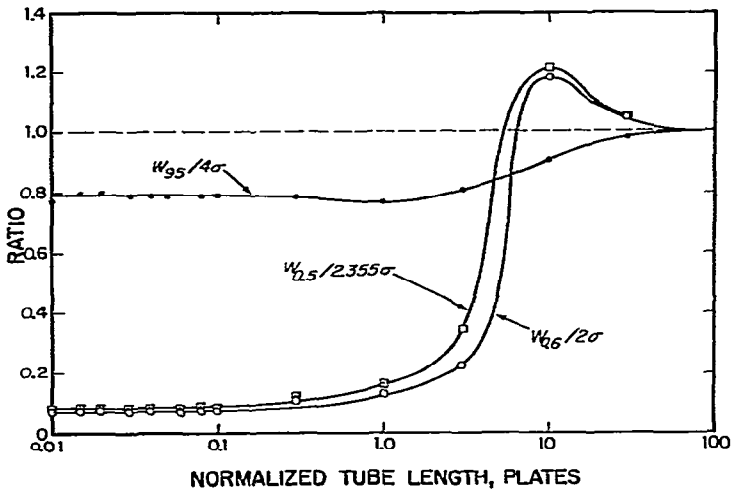

Fig. 3. Accuracy of commonly used measures of bandwidth in determining the standard deviation of peaks eluted from a straight tube. W_{95} is bandwidth containing 95.46% of peak area. $W_{0.5}$ and $W_{0.6}$ are widths at half and 0.606 of maximum height, respectively. Each measure is divided by its value in terms of the standard deviation, σ, for a gaussian peak. These ratios are plotted *versus* normalized tube length on a log scale. Values are from the numerical computer model.

for a gaussian peak. The fifth column gives $W_{0.6}/2\sigma$. A third measure is "base width", W_{95}, the minimum width containing 0.9546 of the peak area. Though harder to measure than $W_{1/2}$ and $W_{0.6}$, it is easier to measure than true σ, especially when the peak is recorded on a system which can integrate peak area. It equals 4σ for a gaussian peak. The sixth column gives $W_{95}/4\sigma$. Fig. 3 shows these three ratios plotted *vs.* tube length in plates.

These results show that $W_{1/2}$ and $W_{0.6}$ give reasonable values down to $n = 10$ plates, but for shorter tubes become an extremely unreliable measure of σ. Below 0.3 plates, when the early part of the peak has adopted its sharp onset and hyperbolic decay, both measures again assume a fixed ratio with the true σ.

For $n = 0.1$ plates, these ratios are

$$W_{1/2} \approx \sigma/12 \tag{6}$$

and

$$W_{0.6} \approx \sigma/14 \tag{7}$$

W_{95} varies much less with n than the others. For $n \leqslant 0.3$ plates,

$$W_{95} \approx 0.79\sigma \tag{8}$$

and for $n \leqslant 4$ plates, eqn. 8 is still accurate to 3%.

Peak location and centroid

It is common to estimate the "dead" volume of a tube or column by measuring

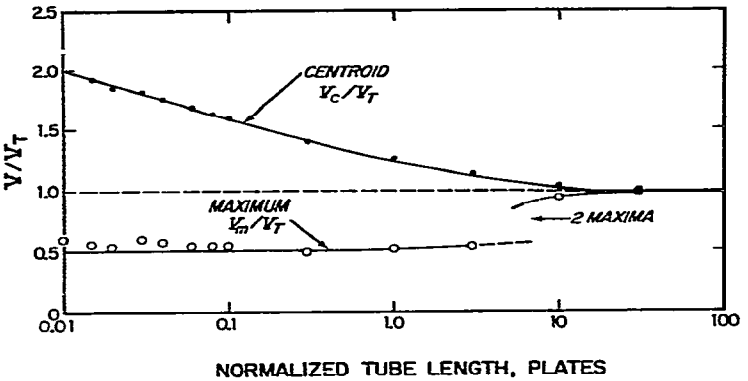

Fig. 4. Retention volume of the centroid V_c and the maximum V_m of elution peaks from the numerical computer model of a straight tube *versus* tube length. Normalized retention volumes V_c/V_T and V_m/V_T are plotted *versus* normalized tube length, n, in plates on a log scale. Above 10 plates, both curves are asymptotic to 1.0. For lower plates, the centroid becomes increasingly delayed owing to the tail caused by slow moving sample near the wall. The peak has two maxima between about 3 to 10 plates. For shorter tubes the correct theoretical maximum is extremely close to the onset at $V/V_T = 0.5$. Values above 0.5 for $0.01 \leqslant n \leqslant 0.1$ plates show errors caused by the coarseness of the model for early events.

the delay between injection into it and elution of a peak from it at a known flow-rate. This method implies an assumption that there has been sufficient velocity averaging so that the injected peak has traveled at the average flow-rate in the tube. In straight open tubes where $n < 30$ plates, this condition is not true. Fig. 4 is a plot of the normalized retention volumes of the eluted peak's maximum V_m/V_T and its centroid, V_c/V_T as a function of tube length in plates. Data for the centroid are in the seventh column of Table II.

Above a length of 10 plates, the eluted peak has a single maximum near V_T. Between 10 and 3 plates, the peak has two maxima, one near V_T and one near $V_T/2$. Below 3 plates, the location of the maximum approaches $V_T/2$ very closely, as expected by the simple theory. That the computed values of V_m below 0.1 plates lie slightly above $V/V_T = 0.5$ can be ascribed entirely to the aforementioned coarseness of the model for the very earliest events.

The centroid on the other hand, is predominately determined by the center and long tail of the peak, which are more accurately computed than the peak maximum, even for the shortest tube. Fig. 4 shows that for $n < 10$, the centroid of the eluted peak becomes delayed to far beyond $V/V_T = 1$. For a tube 0.01 plates long, a large error will be made by estimating its volume to be equal to the retention volume of the eluted peak. The estimate will be a factor of 2 low if the peak maximum is used, and a factor of 2 high if the centroid is used as the measure of retention.

Slice content peaks

Some detectors respond to the total sample content of a slice across the tube, regardless of the radial location or longitudinal velocity of the sample within the slice. An example is a fluorescence detector whose beam crosses a transparent segment of the tube, and responds to concentration of the sample.

Fig. 5 shows the peak shapes seen by detectors that respond to slice content in

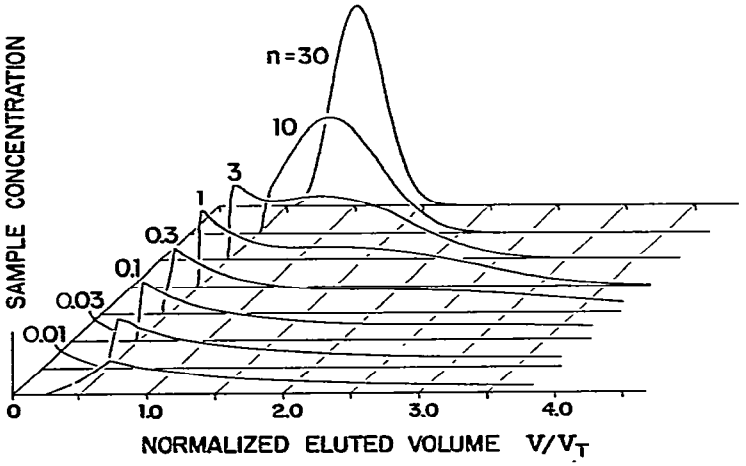

Fig. 5. Slice content peak shapes as a function of normalized tube length, n, in plates. Computed average sample concentration in the last slide of the tube is plotted *versus* normalized retention volume. Normalizations are the same as for the elution peaks of Fig. 1. Slice content peaks are broader and show a more pronounced development of the transition hump than the corresponding elution peaks because relatively greater weight is given to the slowly moving sample near the tube wall where the hump develops.

the slice at the end of the tube for tubes from 0.01 to 30 plates in length. The abscissa scales are normalized in the same way as for the elution curves of Fig. 1 to represent tubes of constant volume. The ordinate scales are set to simulate the same mass of sample injection for all peaks.

Just as for elution curves, the slice content curves for $n < 3$ plates should all rise abruptly to a peak at $V/V_T = 0.5$. But unlike elution curves, they should then decline with a hyperbolic form $(V/V_T)^{-1}$ until the passage of the hump. Except for

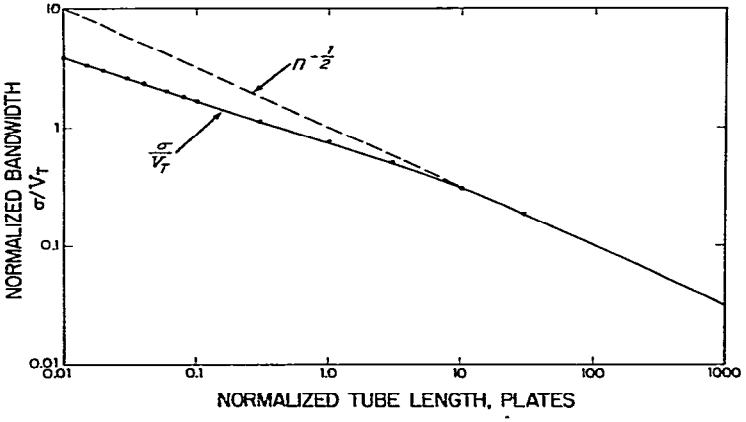

Fig. 6. Slice content bandwidth *versus* tube length on log–log scales. Normalized standard deviation σ/V_T *versus* normalized tube length n in plates for the peak seen by a slice content detector at the output end of the tube. Solid dots are values from the numerical computer model. Broken line shows extension of $n^{1/2}$ asymptote which applies for $n > 30$.

TABLE III

PROPERTIES OF THE SLICE CONTENT SIGNAL AT THE END OF A SHORT STRAIGHT TUBE AS A FUNCTION OF NORMALIZED TUBE LENGTH IN THEORETICAL PLATES

Normalized tube length in plates, n	*Normalized standard deviation from computer,* σ/V_T	*Ratio of approximate formula to normalized standard deviation from computer,* $n^{1/2}\,(1 + 8/n)^{-1/7}/(\sigma/V_T)$	*Ratios of other bandwidth measures to standard deviation*			
			Width at half height, $W_{1/2}/2.355\sigma$	*Width at 0.6066 of height,* $W_{0.6}/2\sigma$	*Width containing 0.9546 of peak area,* $W_{0.95}/4\sigma$	*Normalized centroid,* V_c/V_T
0.010	3.864	0.996	0.119	0.0930	0.788	4.470
0.015	3.264	1.020	0.0936	0.0676	0.785	3.927
0.020	2.921	1.028	0.0945	0.0711	0.784	3.640
0.030	2.570	1.010	0.111	0.0856	0.784	3.217
0.040	2.306	1.016	0.120	0.0965	0.785	3.112
0.060	1.992	1.018	0.134	0.106	0.784	2.808
0.080	1.814	1.008	0.139	0.112	0.785	2.645
0.10	1.674	1.008	0.148	0.116	0.787	2.504
0.30	1.131	1.005	0.220	0.174	0.804	1.956
1.0	0.748	0.977	0.727	0.243	0.815	1.547
3.0	0.499	0.959	1.114	1.18	0.845	1.273
10.0	0.302	0.960	1.156	1.13	0.921	1.027
30.0	0.178	0.989	1.05	1.04	0.982	1.033

sloped onsets for the shortest tubes, the computed curves show this form. Their tails are higher and longer than the $(V/V_T)^{-2}$ tails of the elution curves. In slice content peaks, sample near the wall is weighted equally with sample near the axis of the tube, in spite of its slower velocity. Since the sample hump that terminates the tail is largely at the wall in the early stages, its passage in slice content peaks is much more pronounced than in the corresponding elution peaks. Table I shows that the persistence of slice content peaks is always greater than for elution peaks for the same tube, and much greater for very short tubes.

Fig. 6 shows plots of normalized standard deviation σ/V_T *versus* tube length in plates. As for elution, the normalized standard deviation of slice content peaks is also asymptotic to $n^{-1/2}$ for large n, but is approximately proportional to $n^{-0.38}$ for $0.01 < n < 0.3$ plates.

Table III gives computed values for σ/V_T,, $W_{1/2}/2.355\,\sigma$, $W_{0.6}/2\sigma$, $W_{95}/4\sigma$ and V_c/V_T. These results show that for slice content peaks, $W_{1/2}$ and $W_{0.6}$ are also poor measures of bandwidth, while W_{95} bears nearly the same ratio to true σ as it does for elution peaks. For slice content peaks, the centroid is delayed more than twice as much as for elution peaks.

An approximate empirical formula for σ/V_T for slice content peaks is

$$\sigma/V_T \approx n^{-1/2}\,(1 + 8/n)^{-1/7}, \qquad n \geqslant 0.01 \tag{9}$$

Over the range $n \geqslant 0.01$ it agrees with computed results to within 4.1 %, as shown in Table III. As for eqn. 5 eqn. 9 is completely empirical, and there is no justification for extending it to values of n below 0.01.

Curved tubes and inertial mixing

If a tube is not perfectly straight, smooth, and of uniform cross section, then at high flow-rates, an inertial flow may develop in it. This may cause radial mixing in addition to that caused by diffusion alone. If this additional radial mixing is significant compared to that caused by diffusion, then the straight tube theory will not apply. In LC systems this occurs while the Reynolds number is still too small for true turbulence, and both the main and secondary flows are laminar.

Since the radial mixing effect of inertial flow generally increases rapidly with increasing flow-rate, while the mixing effect of diffusion alone does not, we can expect there to be a transition flow-rate, F_{trans}, at which the inertial mixing effect becomes significant compared to diffusion.

When the tube is coiled into a helicoidal path, the centrifugal force on the faster flowing fluid on the tube's axis causes it to drift radially outward from the center of the curved path. This gives rise to a secondary flow superposed on the Poiseuille flow which divides it into two kidney-shaped counter-rotating circulations in the plane normal to the tube's axis. Under these conditions, the secondary flow will cause a decrease in the plate height, and at the transition flow-rate, the fractional plate height reduction will be proportional to the fourth power of the main flow-rate, as determined by Golay[6]. Using his eqn. 35 for the diffusion constant, k:

$$k = D + \frac{v_0^2 r_0^2}{48D}\,(1 - 18.43\sigma^2) \tag{10}$$

this fractional decrease is given by his term $18.43\sigma^2$, wherein, from his eqn. 23 σ designates the dimensionless quantity

$$\sigma = \frac{\varrho v_0^2 r_0^3}{525\, D\mu r_1} = \frac{\varrho F^2}{525\, \pi^2 D\mu r_0 r_1} \tag{11}$$

where r_1 is the radius of its helicoidal path, μ is the mobile phase's viscosity and ϱ its density. Defining the transition point as that at which σ has the value 0.1, for which we would have an 18 % decrease in plate height, we derive the transition flow-rate as

$$F_{trans} = (518\, r_1 r_0 D\mu/\varrho)^{1/2} \tag{12}$$

The same relationship can be derived from Tijssen[7] (Table I, eqn. 1) by setting his $D_r/D_m = 1.1843$ and solving for flow-rate. The coefficient resulting within the parentheses is 491, which is in substantial agreement with eqn. 12.

It is worth noting that with any likely tube curvature in an LC system, the transition flow-rate, F_{trans}, will be much less than the flow-rate at which turbulence will occur which is for a Reynolds number of the order of 2000, *i.e.*, for a flow-rate given by

$$F_{turb} \approx 1000\, \pi\mu r_0/\varrho \tag{13}$$

Setting $F_{trans} = F_{turb}$, we determine for r_1:

$$r_1 \approx \frac{(1000\, \pi)^2}{518}\left(\frac{\mu}{\varrho D}\right) r_0 \tag{14}$$

For the dimensionless ratio $\mu/\varrho D$, the lowest reasonable value in LC mobile phases is about 10^2, so we obtain

$$r_1 \approx 2 \cdot 10^6\, r_0 \tag{15}$$

Even for a very small tube with $r_0 = 0.05$ mm, the radius of curvature r_1 would be about 100 m. For all such tubes less straight than this, as flow-rate is increased, transition flow would occur at a lower flow-rate than turbulence.

In the case of the continuously curved tube, the inertial mixing occurs uniformly throughout the length of the tube, as does diffusion mixing. However, significant inertial mixing can also occur at single locations in a tube, such as sharp bends, step changes in diameter, or internal projections which partially block the cross section of the tube.

The mixing effect of features such as these will also increase rapidly with the flow-rate so that when they are present, a transition flow-rate will exist beyond which experimentally determined plate heights may be markedly lower than predicted by the straight tube theory.

EXPERIMENTAL AND RESULTS

Measurements on a straight tube

The peak shapes and bandwidths eluted from a straight tube of fixed length were measured over a wide range of flow-rates. In this way the normalized length of the tube was varied by varying the flow-rate only.

A 366 cm × 1/16 in. O.D. × 0.38 mm (0.015 in.) I.D. stainless-steel tube was fastened to a groove in a long wood beam so that it was maintained straight within about 5 mm over its entire length. Samples were injected into the tube using a Rheodyne Model 7120 valve with an injection loop modified to deliver 6 μl, and connected to the straight tube with about 10 cm of 0.18 mm I.D. tube and an SSI (State College, PA, U.S.A.) low dead-volume union. The peaks eluted from the tube were measured by a specially made 3 × 1 mm I.D. UV flow cell, with a volume of about 2.6 μl, connected to the straight tube by about 25 cm of 0.18 mm tube and 2 SSI unions. The cell was mounted in a Perkin-Elmer Model LC-55 UV detector set at 254 nm. Output peaks were recorded on a strip chart recorder. The mobile phase was deionized water pumped by a Perkin-Elmer Series 2 pump. Flow-rates were measured by timing collection of effluent in a graduated cylinder. The samples injected were 0.1 or 0.2% sodium benzoate in water. At each of 11 flow-rates, from 0.105 to 4.16 ml/min, at least two injections were recorded. Recorded peaks were digitized on a Bendix Datagrid (Fairfield, CT, U.S.A.) and processed to obtain bandwidth measures by the same program used to process peaks generated by the computer model described above.

The length of the tube was chosen so that at the three lowest flow-rates used, 0.105, 0.21 and 0.31 ml/min, its normalized length was over 30 plates, and the eluted peaks were nearly gaussian. This made it possible to measure the tube volume accurately by measuring the retention volume V_c of the centroid of the eluted peak. Also it permitted a determination of the actual sample diffusivity by measuring the peak spreading in the tube under conditions where the long tube theory of eqns. 3 and 4 applied. Knowledge of the diffusivity was necessary to determine n, the normalized tube length in plates, at higher flow-rates where n cannot determined directly from the peaks themselves because of their extreme departure from gaussian shape.

First, the instrumental contribution to retention volume, V_I, and standard deviation σ_I were determined by replacing the 366-cm tube with a short segment of 0.18 mm I.D. tube having negligible volume contribution, and recording the output peaks at the same flow-rates. At the three lowest flow-rates, the instrumental retention volume V_I varied little and averaged 42 μl. With the 366-cm tube in place, the average difference between the total retention volume V_c and the instrumental retention volume V_I measured at the three lowest flow-rates gave a value of tube volume V_T of 485 μl. This corresponds to an inside diameter of 0.41 mm, 8% above the nominal for the tube. This value for V_T was used in normalizing all measurements on the 366-cm tube.

To determine sample diffusivity, two measurements of σ corrected for instrumental contribution σ_I were made at each of the three lowest flow-rates used. From each of these σ measurements, a plate height, h, in the tube was calculated, using eqn. 4 to calculate n in eqn. 3. The results are shown in Table IV.

From eqn. 2, under conditions where the long tube theory applies, and S is the

TABLE IV

MEASURED PLATE HEIGHT *VS.* FLOW-RATE FOR 366-cm STRAIGHT TUBE

Sample was 0.1 % sodium benzoate in water at 24°C. These data were used to determine the diffusivity of sodium benzoate to be $8.1 \cdot 10^{-6}$ cm²/sec.

Flow-rate, F (ml/min)	*Plate height, h (cm)*	
	First run	*Second run*
0.105	4.3	3.3
0.21	7.6	6.1
0.31	7.1	7.7

slope of the straight line which passes through the origin and relates plate height to flow-rate:

$$D = 1/24\,\pi S \tag{16}$$

A least squares best fit straight line passing through the origin was fitted to the data of Table IV and its slope was determined. From eqn. 16, D was found to be $8.1 \cdot 10^{-6}$ cm²/sec. This value of diffusivity was used in analyzing all experiments with sodium benzoate sample in water mobile phase. As a check on its reasonableness, it may be compared with the value of $9 \cdot 10^{-6}$ cm²/sec for toluene, a molecule of similar size, in water at 20°C given by Bristow[9].

Using the measured value of D and eqn. 3, n was found for each flow-rate. The measured σ at each flow-rate was normalized by the measured tube volume, V_T. The results are plotted on Fig. 2, to compare them with the values predicted by the computer model.

Measurement of transition flow in a curved tube

The 366-cm tube described above was removed from its straight wooden support and coiled into a circle of radius $R = 56$ cm. Eluted peaks were recorded at 6 flow-rates from 0.105 to 4.16 ml/min and their standard deviations were measured. Fig. 7 shows a plot of the normalized measured standard deviations *vs.* flow-rate. Also shown for comparison are the theoretical values for this tube calculated using the measured V_T, D and F in eqn. 3 to obtain n, then using the approximate formula of eqn. 5 to calculate σ/V_T.

It can be seen that at and below about 0.5 ml/min, the measured bandwidth agrees well with the straight tube theory, but above this flow-rate it becomes lower. At 4 ml/min, it is half that predicted for a straight tube. The calculated transition flow-rate for this tube using eqn. 12 is $F_{trans} = 0.38$ ml/min.

Fig. 8 shows comparison of the peak shapes at the same flow-rate for the straight tube and the same tube curved to 56 cm radius. The effect of curving the tube is to delay and slope the sharp onset of the typical short-tube peaks, truncate the tail and make the profile much more gaussian. Ref. 4 showed that in short tubes the sharp onset is caused by sample on the tube axis while the tail is from sample at the wall, so these changes in peak shape indicate that radial mixing has occurred.

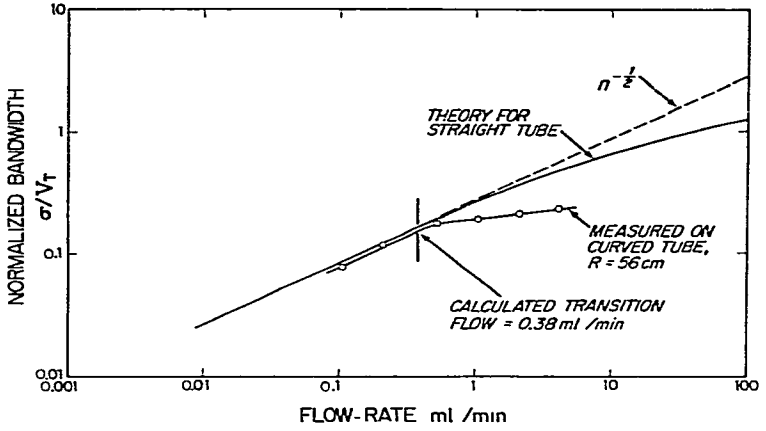

Fig. 7. Bandwidth *versus* flow-rate for a curved tube on log–log scales. Normalized bandwidth σ/V_T *versus* flow-rate for a tube 366 cm long with sodium benzoate sample in water mobile phase at room temperature. Solid curve is calculated from eqn. 5 for the tube when straight. Broken line is extension of asymptote applicable when $n > 30$. Circles are measurements made when the tube was curved into a circular path with radius 56 cm. Arrow indicates the transition flow-rate above which theory for straight tubes does not apply, calculated from eqn. 12.

In another experiment the 366-cm tube was folded into a "hairpin" shape with a 180° bend of 10 cm radius between two straight segments 167 cm long. In this shape, the tube's bandwidth obeyed straight tube theory up to a flow-rate of about 0.7 ml/min, but departed at higher flow-rates with bandwidth only 0.6 of that for the straight tube at 2.08 ml/min.

Measurements on a fluorescence flow cell

To study the applicability of the computer model to very short tubes, measurements were made on an experimental flow cell for a fluorescence LC detector. The flow cell consisted of a cylindrical fused-silica tube (8 × 1.5 mm I.D.). At each end of

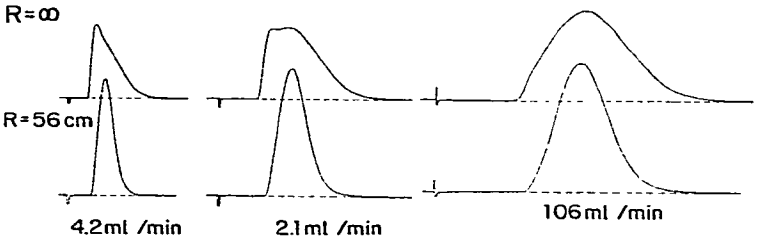

Fig. 8. Effect of curved path on eluted peak shape. Measured peak shapes eluted from a stainless-steel tube (366 cm × 0.38 mm I.D.) at three flow-rates. For upper curve of each pair (marked $R = \infty$), the tube was straight. For lower curve, the same tube was coiled in a circular path of radius $R = 56$ cm. Sample was sodium benzoate in water at room temperature. These peak shapes for the curved case are from among the runs averaged to obtain the three corresponding experimental points plotted in Fig. 7. Though the radius of the curved path was about 1700 times the radius of the tube, curvature reduced the standard deviation of the eluted peak more than a factor of 2 at 4.2 ml/min. Repeated curving and straightening of the same tube showed that these peak shapes and bandwidth effects were quite reproducible.

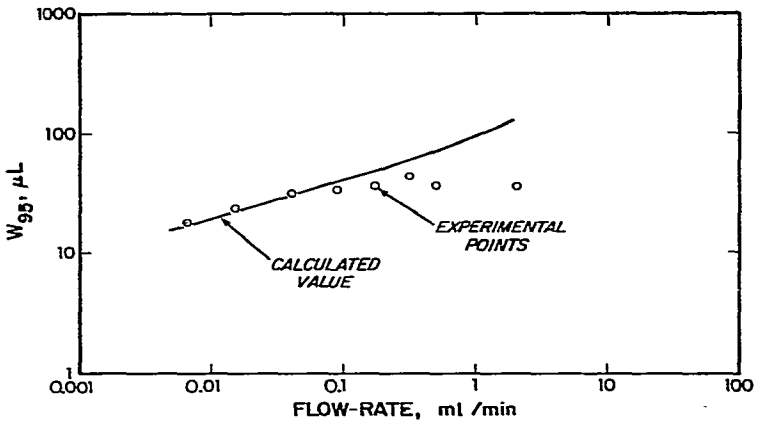

Fig. 9. Bandwidth of a fluorescence flow cell *versus* flow-rate. Measured bandwidth containing 95% of the peak area, W_{95}, is plotted *versus* flow-rate on log–log scales. The cell had 1.5 mm I.D. and was 8.5 mm long. The excitation and fluorescence beams intersected at a focus 4.3 mm from the cell entrance. Sample inlet was axially via a 0.38 mm diameter tube and a conical transition piece of 90° included angle. Cell volume from inlet to beam focus was 7.5 µl. Sample was naphthalene in isopropanol. Calculated curve is from eqn. 9 and assumed the cell acted as a slice content detector. Bandwidth lower than calculated at high flow-rates may be evidence of inertial mixing at the junction of the inlet tube and cell entrance.

this silica tube, an entrance or exit tube of 0.38 mm I.D. connected to it coaxially with a conical transition piece of 90° included angle. The optical excitation and fluorescence beams crossed at the center of the cell. Their images were about 1.5 mm high and 1.5 mm wide, effectively filling the cross-section of the cell.

The mobile phase was isopropanol. The sample was naphthalene at 0.5 to 2 µg/ml in isopropanol. The experimental fluorimeter was set for 280 nm excitation and 340 nm fluorescence with 10 nm spectral slit width in both beams. Pumps used were a Perkin-Elmer Series 2 for flow-rates from 2 to 0.2 ml/min, and a specially modified version of the same pump with smaller piston and stroke below 0.2 ml/min. A Valco injection valve with 0.5-µl loop was connected to the detector with 10.5 cm of nominal 0.007 in. stainless-steel tubing and an SSI union. Measurements were made at 8 flow-rates from 0.0065 to 2.0 ml/min. Three to five injections were recorded at each flow-rate on a Bascom Turner recorder. The integrating feature of the recorder was used to determine W_{95}, the bandwidth containing 95.46% of the peak area. The results are shown in Fig. 9.

The theoretical bandwidth of the detector was calculated as follows. The cell was treated as a tube 1.5 mm in diameter with a uniform injection over its input end, and a slice content detector 4.25 mm from the input. Its tube volume was calculated to be 7.5 µl. The diffusivity of naphthalene in isopropanol was estimated to be $4.1 \cdot 10^{-6}$ cm^2/sec by multiplying published values in methanol and benzene[9] by the ratios of the viscosities of those solvents to the viscosity of isopropanol. The normalized length at each flow-rate was calculated using eqn. 3. It ranged from 1.21 plates at 0.0065 ml/min to 0.0039 plates at 2 ml/min. At 0.01, 0.1 and 1 ml/min, the σ for the cell was calculated using eqn. 9 for slice content detectors, and corrected for the error of this expression by interpolation from column 3 of table III. Then W_{95} was calculated by multiplying by the tabulated ratio $W_{95}/4\sigma$ from column 6. Similar calcu-

lation of the elution bandwidth of the connecting tubes show that their contribution should range from a W_{95} of about 2 μl at 0.01 ml/min to about 4 μl at 1 ml/min even if they were straight, which they were not. The contribution of the 0.5-μl injection value was previously measured and found insignificant. Therefore their contributions were ignored. The calculated results are plotted on Fig. 6 for comparison with the measured values.

Measurements on tubes of varying length at fixed flow-rate

Four different straight lengths of a nominal 0.007 in. I.D. stainless-steel tube were connected between the injection valve and the detector of an LC instrument system and the bandwidth contribution of the instrument and of each length of tubing were determined.

The instrument consisted of a Perkin-Elmer Series 2 pump, a Valco injection valve with 0.5-μl loop, a Perkin-Elmer Model LC-75 UV detector with flow cell (3 × 1 mm I.D.) with a volume of about 2.6 μl, but slightly different design than that described in the previous experiment.

First a 100-cm straight length of 0.007-in. tube was put in place, several injections were made, and the detector signal was recorded. Then, a 25-cm length was cut from this tube, leaving 75 cm of the original tube. A new ferrule was mounted on it and the 75-cm piece was reconnected in place and more injections were made. This process was repeated leaving 50-, then 25-cm lengths of tubing in place. For each length of tubing, three to five injections were recorded. The flow-rate was measured to be 0.5 ml/min.

Data were processed as follows. First, the actual volume of each length of tube was determined as shown in Table V. It was assumed that each 25-cm segment of tube had the same unknown volume, V_{25}, and that the instrument alone contributed a fixed volume with centroid V_I in all the measurements. It was also assumed that the centroid of the instrumental contribution V_I and of the peak eluted from each tube, V_c, added to give the measured centroid in each experiment. The mean measured centroid is given in the third column of Table V with 90% confidence limits calculated from the measured standard deviations and Student's t factor[10].

From Fig. 4, the ratio of V_c to V_T for each tube was determined. Using it, an equation relating measured centroid, instrumental centroid, and tube volume was written as shown in the fifth column of Table V. Three independent solutions from the four equations gave mean values of 25.9 μl for V_I and 7.56 μl for V_{25}. The volume of each tube was taken to be the appropriate multiple of V_{25}. They correspond to an inside diameter of 0.196 mm (0.0077 in.), 10% larger than nominal.

The mean variance measured for each tube length is shown in the fourth column of Table VI, with 90% confidence limits calculated from the standard deviation of the measurements and Student's t factor. It was assumed that each mean variance was the sum of the fixed instrumental variance σ_I^2 plus the variance of the tube. Using the measured tube volumes and eqn. 5 the variance of each tube was calculated as shown in the sixth column of Table VI. The instrumental variance was determined as the single value which when added to the four calculated tube variances gave the least squares best fit to the four measured mean variances. This instrumental variance was 66.3 μl^2. The difference between it and each measured total variance was taken as the variance of each tube from measurements. This is compared in column 5

TABLE V

DETERMINATION OF TUBE VOLUMES FROM MEASUREMENTS

Change in measured centroid with change of tube length is corrected by delay ratio V_c/V_T for centroid of short tubes. V_1 is the centroid volume of the instrument alone, assumed to be fixed. V_{25} is the true volume of a 25 cm segment of the tube, assumed to be uniform for all lengths of tube. Tube volume is the average of 3 independent determinations from the four equations. Average value for V_1 is 25.9 μl.

Tube length (cm)	*Normalized length in plates (n)*	*Measured centroid of instrument plus tube, with 90% confidence limits (μl)*	*Delay ratio of centroid to tube volume, V_c/V_T from Fig. 4*	*Equation relating measured centroid to instrumental centroids and tube volume*	*Tube volume, V_T determined from simultaneous equations (μl)*
100	7.34	57.6 ± 1.5	1.04	$57.6 = V_1 + 1.04\,(4V_{25})$	30.2
75	5.50	50.0 ± 0.6	1.07	$50.0 = V_1 + 1.07\,(3V_{25})$	22.7
50	3.67	42.2 ± 0.7	1.11	$42.2 = V_1 + 1.11\,(2V_{25})$	15.1
25	1.835	35.1 ± 0.6	1.17	$35.1 = V_1 + 1.17\,(1V_{25})$	7.56

TABLE VI

COMPARISON OF MEASURED AND THEORETICAL BANDWIDTHS FOR FOUR SHORT TUBES

Four different lengths of nominal 0.007-in. diameter straight tube measured in a UV instrument system with an estimated instrumental variance of 66.3 μl^2. Sample is sodium benzoate in water mobile phase at room temperature.

Tube length, (cm)	*Calculated normalized length in plates (n)*	*Tube volume from centroid measurements, V_T (μl)*	*Measured variance of tube plus instrument, with 90% confidence limits (μl^2)*	*Variance of tube*		*Standard deviation of tube*	
				From measurements, σ^2 (μl^2)	*Theoretical, from eqn. 5, σ^2 (μl^2)*	*From measurements, σ (μl)*	*Theoretical, from eqn. 5, σ (μl)*
100	7.34	30.2	163.8 ± 26.2	97.5	104.7	9.9	10.2
75	5.50	22.7	146.0 ± 5.1	79.6	75.4	8.9	8.7
50	3.67	15.1	119.9 ± 13.3	53.6	46.1	7.3	6.8
25	1.84	7.6	81.2 ± 2.2	14.9	19.1	3.9	4.4

TABLE VII

BANDWIDTH OF TUBES JOINED BY UNIONS

A total length of 100 cm of nominal 0.007-in. tube divided into segments joined by unions, and measured in a UV instrument system with an estimated instrumental variance of 66.3 μl^2. Sample was sodium benzoate in water mobile phase at room temperature.

Length of tube segments joined by unions (cm)	*Measured variance of joined tubes plus instrument, with 90% confidence limits (μl^2)*	*Variance of joined tubes*		*Standard deviation of joined tubes*	
		From measurements (μl^2)	*Theoretical from col. 6, Table V (μl^2)*	*From measurements (μl)*	*Theoretical from col. 4, this table (μl)*
100	164.8 ± 26.2	98.5	104.7	9.9	10.2
75, 25	155.0 ± 15.9	88.7	94.5	9.4	9.7
50, 25, 25	150.0 ± 4.7	83.5	84.2	9.1	9.2
25, 25, 25, 25	138.8 ± 1.7	72.5	76.4	8.5	8.7

of Table VI. Standard deviations of the tubes from measurement and theory are the square roots of these variances shown in columns seven and eight.

Measurements on coupled tubes

The effect of breaking a single straight tube into an assembly of shorter segments coupled with unions was studied as follows. During the performance of the previously described experiment on tubes of varying length, after each 25-cm segment was cut from the initially 100-cm tube, it was joined again to that tube with an SSI union, together with all other 25-cm segments previously cut off, so that the overall length was still 100 cm. Several injections were made and peaks were recorded. All conditions were otherwise the same as in the previous experiment. This resulted in measurements on 100 cm of tube in these four configurations: one piece, 100 cm; one piece 75 cm, one piece 25 cm and one union; one piece 50 cm, two pieces 25 cm and two unions; four pieces 25 cm and three unions. The means of variances measured on each configuration, with 90% confidence limits are shown in the second column of Table VII.

The variance of each tube configuration was determined by subtracting from the mean total variance the 66.3 μl^2 instrumental variance determined in the previously described experiment with tubes of varying length. The results are shown in the third column of Table VII. In the fourth column the theoretical variance for each configuration is given. It was calculated by adding the theoretical variances of the appropriate components previously calculated and given in the sixth column of Table VI, and ignoring the contribution of the unions. For example, the theoretical variance for the combination of 50-, 25- and 25-cm pieces is the sum of the calculated variance for the 50-cm tube plus twice the calculated variance of the 25-cm tube from Table VI. The corresponding standard deviations from measurement and theory are compared in the fifth and sixth column of Table I.

DISCUSSION

Applicability of the results for straight tubes

In the experiments on the 366-cm tube, its normalized length ranged from 126 down to about 3 plates. Though the predicted doubly curved peak shapes were observed in the transition region near 10 plates, this is an insufficient range of n to show conclusively that the experimental results agree with the results of the computer model. However, the good agreement of the measurements on the fluorescence detector with the predictions for low flow-rates suggests that the results of the computer model apply to very short tubes. Long tube theory applied to the fluorescence cell would predict a minimum bandwidth contribution 2.5 times greater than observed at 0.1 ml/min.

We speculate that the measured bandwidths of the fluorescence cell which are much lower than predicted at high flow-rates are caused by an inertial mixing effect at the junction of the 0.38 mm diameter lead-in tube and the 1.5 mm diameter cell. Rough calculations show that at 0.1 ml/min, the kinetic energy of the liquid leaving the lead-in tube is more than adequate to sustain a toroidal secondary circulation in the initial part of the cell. This circulation may extend 1 or 2 tube diameters into the cell. Since the cell's length from entrance to detector beam is less than 3 tube diameters, such an inertial mixing process could be expected to substantially reduce its bandwidth. Just as for other inertial mixing effects, it should exhibit a transition flow-rate. If this is true, the experimental data suggest that the transition flow-rate is of the order of 0.05 ml/min in this case.

Curved tubes

Measurements on the curved 366-cm tube confirm the applicability of the transition flow eqn. 12. No effort was made in this work to study quantitatively the bandwidth of curved tubes at higher than the transition flow-rate.

Significant findings are the surprising sensitivity of bandwidth of connecting tubes to slight curvature, and that a single bend functions as a localized mixing feature at flow-rates common in LC systems. These results mean that in practical LC systems so much of the tubing is operated above its transition flow-rate that its contribution to extra-column bandwidth is generally much less than straight tube theory would predict, except at the very low flow-rates used with microbore columns[8].

Additivity of variances

A uniform tube can contribute a variance proportional to its length if and only if the variance of any segment of the tube obeys eqn. 4, the long-tube case. In the results of the computer model for short tubes where $n < 30$ the variance departs increasingly from eqn. 4. Therefore, according to the model the variances of successive short segments of a tube do not add.

The results of the experiment with four tubes of different length reported in Tables V and VI, are consistent with the results of the computer model, but they may not be proof of the non-additivity of variances because, within the errors of the assumptions and measurement, other interpretations may be possible. But this experiment established reasonable values for the tube volumes and the instrumental

variance used in the parallel experiment on the effect of unions on the bandwidth of 1 m of tube reported in Table VII. In this parallel experiment, it was clearly shown that the sum of the measured variances of separate segments of tube joined by unions is less than the measured variance of the same segments when in one continuous piece. This is in agreement with the computer model's results for short tubes.

An explanation of the bandwidth-reducing effect of unions is as follows. A necessary condition for variances of successive components in a flow path to add is that the concentration of sample entering and leaving each component must be describable by a single-valued function of time. This is not the case for short segments of open tube smoothly joined together to form a continuous piece. Sample injected on the axis of a short segment is eluted close to the axis. Sample injected near the wall is eluted much later, near the wall. Even in a very long straight tube, when a sample is injected uniformly and simultaneously over the entrance to the tube, it emerges at the end with the sample distribution on the axis leading the distribution at the wall by 3 theoretical plates. Because of this, the variance of a segment which is connected as a continuation of the tube will be additive to the variance of the original tube only if the normalized length of the continuation is much greater than 3 plates. Then the spread of 3 plates between axis and wall as the sample enters the continuation will be negligible compared to the spreading effect of the continuation segment itself.

If the second segment is added not as a continuation of the first tube, but is coupled to it with a union, the union may act as a localized mixing feature which thoroughly mixes sample from the axis and the walls of the first segment of tube and redistributes it uniformly over the entrance to the following segment, without adding significant spreading of its own. Any such localized mixing component causes a transfer of sample from one segment to the next which is describable by a single-valued function of time. Therefore, variances of tube segments joined by such mixing components should add, no matter what the normalized length of the segments.

The experimental results of Table VII show that the measured total variances of the tubes segmented by unions approximately equalled the sum of the variances of their separate segments. This is consistent with the assumption that at 0.5 ml/min, each union functioned as a localized mixing component.

Within the errors of measurement, there was no evidence that the unions contributed variance that was significant compared to the variance contribution of a 25-cm segment of the tube. Since the nominal volume of the through hole in these unions was of the order of 0.2 μl, this is a reasonable result.

It is very likely that most of the radial mixing process in the union is inertial, caused by step changes in cross section or by misalignment. Hence there is probably a transition flow-rate below which the union becomes relatively ineffective as a mixing component. Therefore, one can speculate that in systems used with microbore columns with much lower flow-rates and instrumental bandwidth, the variance contribution of such unions may be higher, their mixing effectiveness lower, and their contribution to instrumental bandwidth no longer negligible.

An ideal column end fitting should also function as a radial mixing component. At the input, it should mix sample from the axis and the wall of a small-bore connecting tube and distribute the resultant fluid uniformly and simultaneously across the top of the column without adding significant variance. At the output of the column, it should perform a corresponding transfer of sample mixture from axis and wall of the

column uniformly and simultaneously cross the entrance to the connecting tube.

Ideal end fittings could have an important effect in joining together a set of packed columns that share a defect which permits samples to travel at a different velocity on axis than at the wall, especially if these columns are short compared to the length that permits radial dispersion to redistribute sample uniformly over the cross-section. The variances of the peaks eluted from these columns should add if they are coupled in series with ideal column fittings and short connecting tubes of negligible bandwidth contribution. But if the columns are coupled in series by removing the end fittings and butting their ends in drilled out unions, it can be expected, for the same reasons as for short open tubes, that their variances should not add, and that the variance of the combination should be greater than the sum of the variances measured on separate segments between column end fittings. Golay[11] proposed mixing devices similar to a pair of ideal end fittings, but internal to the column for large preparative gas chromatographic columns.

Use of a long straight tube to determine diffusivities

When the diffusivity of an LC sample in a particular mobile phase is not known, a convenient method to determine it is to use an LC instrument system to measure the spreading of the sample peak injected into a long straight tube between injection valve and detector. The method should be accurate if precautions are taken against mixing effects other than diffusion, and the tube is long enough so that the long-tube theory applies. These conditions are assured if the measured plate height in the tube is accurately proportional to flow-rate over at least a 2 to 1 range of flow-rates.

To achieve this the tube must be smooth and in a single piece, and straight enough so that F_{trans} calculated using eqn. 12 is substantially larger than the largest flow-rate at which measurements will be made. It must be long enough so that at the highest flow-rate and for the diffusivity being measured, its normalized length is greater than 30 plates. This will generally require physically separating the injection valve from the detector so that they can be connected to the opposite ends of the long tube with short connections. Naturally, the eluted peaks from the tube should have variances at least an order of magnitude greater than that of the instrumental system alone, so that no significant error is caused by correcting for the instrumental volume and variance. This can be measured by replacing the long tube with a very short tube of small diameter having negligible volume and variance contribution.

Axially illuminated absorbance flow cells

The results presented in this paper do not apply directly to axially illuminated flow cells such as are typical in Ultraviolet absorbance detectors. In these cells the sample is injected at one end of the cell and remains fully in the beam until it reaches the other end. The detector signal is thus neither an elution curve nor a slice content curve. Instead, it is the initial amount of sample injected into the tube minus the integral of the elution curve from a short tube of the same length and volume as the cell. Curves for axially illuminated cells and their moments can be derived from the results of the computer model reported here by additional data processing. These results will be reported in another paper.

ACKNOWLEDGEMENTS

The computer numerical models were programmed by Harold Jackson. The programs to analyze results were written by Duncan Harris. The experimental data were taken and reduced by Jane Goldstein. The authors are grateful to these coworkers for their skillful contributions, and to Mrs. Goldstein for conceiving the experiment on the effect of unions.

REFERENCES

1 G. Taylor, *Proc. Roy. Soc. A*, 255 (1956) 67.
2 M. J. E. Golay, in V. J. Coates, H. J. Noebels and I. S. Fagerson (Editors), *Gas Chromatography 1957, (Lansing Symposium)*, Academic Press, New York, 1958, p. 1.
3 W. N. Gill and V. Ananthakrishnan, *AIChE J.*, 13 (1967) 801.
4 M. J. E. Golay and J. G. Atwood, *J. Chromatogr.*, 186 (1979) 353.
5 K. P. Maycock, J. M. Tarbell and J. L. Douda, *Separ. Sci. Technol.*, 15(6) (1980) 1285–1296.
6 M. J. E. Golay, *J. Chromatogr.*, 196 (1980) 349.
7 R. Tijssen, *Separ. Sci. Technol.*, 13 (1978) 681.
8 R. P. W. Scott and P. Kucera, *J. Chromatogr.*, 169 (1979) 51.
9 P. A. Bristow, *Liquid Chromatography in Practice*, hetp, Wilmslow, 1976, p. 250.
10 E. L. Bauer, *A Statistical Manual for Chemists*, Academic Press, New York, 2nd ed., 1971, p. 16.
11 M. J. E. Golay, in H. J. Noebels, R. F. Wall and N. Brenner (Editors), *Gas Chromatography*, Academic Press, New York, 1961, p. 11.